Journal of Optics, 18 (2016) 024007 https://doi.org/10.1088/2040-8978/18/2/024007

Temperature dependent competition between different recombination channels in organic heterojunction solar cells

Theresa Linderl, Ulrich Hörmann, Sergej Beratz, Mark Gruber,
Stefan Grob, Alexander Hofmann, and Wolfgang Brütting*
Institute of Physics, University of Augsburg, 86135 Augsburg, Germany

(Dated: December 1, 2015)

Abstract

A modification of the Shockley-Queisser theory for organic heterojunctions is presented with a special focus on constellations, where a linear extrapolation of the temperature dependence of the open circuit voltage results in the optical gap of the absorber rather than in the intermolecular charge transfer (CT) gap. We demonstrate that, depending on the electronic coupling strength between donor and acceptor molecules, either singlet or CT recombination is dominant in different temperature regimes. The different regimes are separated by a transition temperature that is usually well above room temperature. However, in the case of small energy level offset and weak electronic coupling, it can be around 300 K or even below. We point out that a linear extrapolation of the open circuit voltage V_{OC} towards 0 K for measured temperatures larger than the transition temperature results in a photovoltaic gap that is close to the optical gap, whereas for values below the transition temperature the CT gap will be extracted. We show that for α-sexithiophene (6T)/diindenoperylene (DIP) solar cells heating the substrate during 6T deposition leads to a molecular configuration at the interface where the coupling between donor and acceptor molecules is strongly reduced. This leads to a transition temperature well below room temperature which is confirmed by temperature dependent electroluminescence measurements. By comparing the temperature dependent spectra of high temperature and room temperature grown 6T/DIP solar cells to the spectra of the individual materials, the different contributions from the charge transfer gap and the optical gap are separated.

I. INTRODUCTION

Owing to their light weight and the compatibility with low-temperature fabrication processes on flexible substrates, organic solar cells (OSCs) have the potential for low-cost solar energy conversion with new features like arbitrary shapes, tunable color or high degree of transparency[1,2]. Current record lab cells reach efficiencies in excess of 10 %[3,4], but their thermodynamic efficiency limit is much higher[5]. Using detailed balance arguments, several authors have shown by simulations that the maximum power conversion efficiency, i.e. the electrical power generated by the solar cell per incident solar power, lies in the range of some 20 %[6–8]. Like in inorganic semiconductor cells this number critically depends on the energy gap of the absorber material.

Due to their excitonic nature, however, OSCs require the use of two semiconducting materials, a donor and an acceptor, forming a type-II heterojunction with sufficient energy offset between their highest occupied molecular orbitals (HOMO) as well as their lowest unoccupied molecular orbitals (LUMO)[9]. Charge generation then occurs after photoinduced charge transfer from the initially formed exciton state on the absorber to an intermolecular charge transfer (CT) state at the donor-acceptor interface. This means that there are effectively two relevant gaps in OSCs: (1) the optical gap E_{opt} of the absorber material with the lower gap, because it defines the onset of the photocurrent and (2) the CT gap E_{CT} across which recombination of carrier pairs occurs and which thus determines the open-circuit voltage of the cell. Actually, the radiative recombination of electron-hole pairs via interfacial CT states leading to electroluminescence is one of the established methods to determine E_{CT}[10] and the observed offset between V_{OC} and E_{CT} is a measure for energy losses in OSCs[11].

However, this classical role allocation of the two gaps is not always granted. Faist and Nelson have recently shown by a systematic tuning of the interfacial energy level offset through a variation of the acceptor in polymer:fullerene cells that recombination via the singlet state of the donor competes with CT state recombination for small enough LUMO offsets[12]. Ran and Nguyen found that the observation of singlet exciton electroluminescence in such bulk-heterojunctions also critically depends on the morphology of the donor-acceptor mixed films[13].

Here we use a planar heterojunction of a molecular donor-acceptor pair with α-sexithiophene (6T) acting as donor and diindenoperylene (DIP) as acceptor[14]. Both are rod-shaped

molecules that can be grown as highly ordered thin films with a well-defined molecular orientation. In particular, by using different substrate temperature during film growth one changes the predominant orientation of the molecules with respect to the substrate plane from lying to standing[15]. Thereby, the growth of the DIP acceptor is templated by the underlying 6T donor layer. We are thus able to compare two fundamentally different relative molecular orientations, namely face-on (lying orientation) and edge-on (standing orientation), which were predicted to yield significantly different recombination rates in the case of a pentacene/C_{60} heterojunction[16]. Remarkably, for both orientations of 6T/DIP we found identical interface energy offsets[15], so that this system is ideal for studying effects of intermolecular electronic coupling strength independent of energetic differences, which can lead to ambiguities, if not disentangled properly[17]. Furthermore, in these planar heterojunctions we do not expect such strong morphological impact as in donor-acceptor mixtures[13].

The organization of this manuscript is as follows: In the first part we will use a detailed balance approach to disentangle the influence of singlet exciton and CT recombination on the open-circuit voltage of OSCs and, in particular, on its temperature dependence. The latter is frequently used to assess the magnitude of energy losses of these cells[18,19], but as we show here, this can be misleading under certain conditions. We will demonstrate that, depending on the electronic coupling strength between donor and acceptor molecules, singlet or CT recombination is dominant in different temperature ranges. These different regimes are separated by a transition temperature that is usually well above room temperature, however, in the case of small energy level offset and weak coupling, it can be around 300 K or even below. In the second part, we use temperature dependent electroluminescence spectra of cells with different molecular orientation to demonstrate that the above described scenario does actually occur for standing 6T/DIP at about 250 K, which gives a consistent explanation for the earlier on observed high open-circuit voltage of these cells.

II. SIMULATIONS

The detailed balance limit of a solar cell is a thermodynamic efficiency limit and has first been considered by Shockley and Queisser in 1961.[20] They predicted the thermodynamically possible efficiency of a single pn-(homo)junction to about 33 %. Recently, their model has been extended to describe organic solar cells, where the introduction of an energy offset at

the heterojunction poses an intrinsic energy loss that further reduces the maximum possible efficiency.[6–8,21,22] In the following, these considerations are recapitulated with the focus on the open circuit voltage and how it is affected by the cell temperature.

A. The heterojunction as black body radiator

In this approach, both the sun and the solar cell are regarded as black body radiators at their specific temperatures ($T_s \approx 5778\,\mathrm{K}$ and $T \approx 300\,\mathrm{K}$). In accordance with Planck's law of radiation, the photon flux, i.e. the number of photons per unit area and per unit time, emitted by a black body at temperature T is given by the integral of the black body spectrum over all energies E. To account for the fraction of photons relevant for the photoactive material, the black body spectrum is additionally weighted by the absorption profile of the solar cell, yielding the photon flux that is absorbed by the cell:

$$\begin{aligned} N(T) &= \int_0^\infty \alpha(E) n(E,T) dE \\ &= \int_0^\infty \alpha(E) \frac{1}{4\pi^2\hbar^3c^2} \left(\exp\left(\frac{E}{k_\mathrm{B}T}\right) - 1 \right)^{-1} E^2 dE \end{aligned} \tag{1}$$

Here $\hbar$ is the reduced Planck constant, c the speed of light and k_B is the Boltzmann constant. For an idealized pn-junction, α equals 0 for photon energies below the band gap and 1 for photon energies above the band gap of the semiconductor. Please note that α, strictly speaking, denotes the absorbance and is thus dimensionless. It should not be mixed up with the absorption coefficient, which has the dimension $1\,\mathrm{cm}^{-1}$.

The situation changes slightly for a heterojunction of two different (not necessarily organic) semiconductors: The absorption onset is no longer given by the optical gap of either of the semiconductors in this case. Instead, a charge transfer (CT) process, where an electron is excited from an occupied state of one semiconductor to an unoccupied state of the other semiconductor, enables additional absorption at photon energies below the smallest individual band gap (cf. Figure 1). Thus the absorption profile contains two steps and is

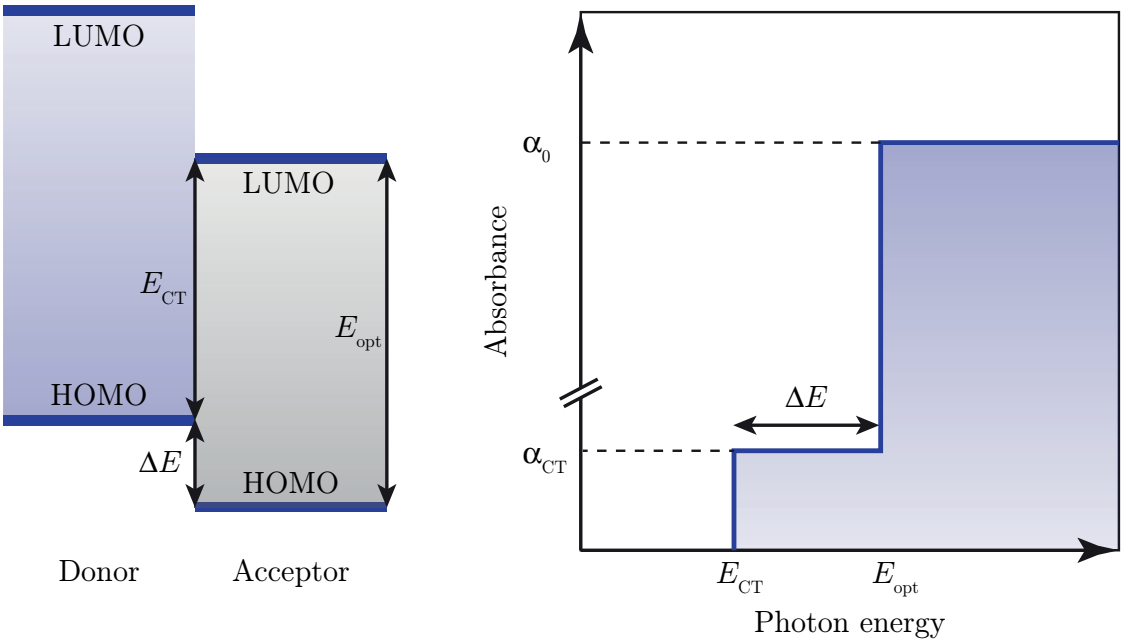

FIG. 1: Schematic illustration of the idealized step absorption profile, resulting from the E_{CT} and E_{opt} energy steps of the donor/acceptor heterojunction.

given by:[6]

$$\alpha(E) = \begin{cases} 0 & : E < E_{CT} \\ \alpha_{CT} & : E_{CT} < E < E_{opt} \\ \alpha_0 \equiv 1 & : E > E_{opt} \end{cases}, \tag{2}$$

where E_{opt} denotes the smaller optical gap of both semiconductors and E_{CT} the charge transfer energy. α_{CT} denotes the absorption strength of the CT transition relative to α_0.

The short circuit current j_{sc} in the radiative limit can now be calculated by Eq. 1 from the number of photons emitted by the sun (approximated as black body radiator at 5778 K) and absorbed by the solar cell. Note that since the sun emits its radiation isotropically into all space, only a fraction of $s = 2.18 \times 10^{-5}$ of the photons reach the surface of the earth.[8] If every absorbed photon generates one electron-hole pair, the short circuit current is given by $j_{sc} = qsN(T = 5778\,\mathrm{K})$, where q is the elementary charge.

On the other hand, Eq. 1 can be used to calculate the photon flux emitted by the solar cell as required by Kirchhoff's law of radiation.[23] The origin of the generation of photons is the recombination of electrons and holes. This may be expressed as a recombination current

for a solar cell at a temperature of 300 K:

$$j_{0,\mathrm{rad}} = qN(T = 300\,\mathrm{K}) \tag{3}$$

This quantity can be extracted as the reverse saturation current j_0 from an ideal device, if radiative recombination, i.e. emission of photons, is the only allowed recombination mechanism. Then, the detailed balance also requires that in equilibrium the amount of absorbed photons equals the amount of emitted photons, if no net current flows. The latter is fulfilled under open circuit conditions. An expression for V_{oc} can be derived from the Shockley equation[24] for an ideal solar cell (ideality factor $n = 1$, series resistance $R_{\mathrm{s}} = 0$ and parallel resistance $R_{\mathrm{p}} \to \infty$) under illumination:

$$V_{\mathrm{oc}} = \frac{k_{\mathrm{B}}T}{q}\ln\left(\frac{j_{\mathrm{sc}}}{j_0} + 1\right) \tag{4}$$

This expression shows that V_{oc} is reduced by the reverse saturation current. Note that j_0 is generally not limited to (thermodynamically inevitable) radiative recombination but usually contains an additional contribution from non-radiative processes, thus that the reverse saturation current is given by

$$j_0 = j_{0,\mathrm{rad}} + j_{0,\mathrm{non}} \tag{5}$$

As a direct consequence, the open circuit voltage of a solar cell is maximal in the radiative limit, i.e. if $j_{0,\mathrm{non}} = 0$. This also implies that an ideal solar cell simultaneously is an ideal light emitting diode, from a photonic point of view[25]. Note, however, that even in the thermodynamically ideal case entropic losses are present caused by the difference of the solid angle under which the sun appears on earth and the solid angle into which emission from the solar cell occurs.[26] In terms of V_{oc} this amounts to an intrinsic loss of about 300 mV compared to the photovoltaic gap.[27–30]

B. The coupling factor

Equation 4 relates the open circuit voltage to the short circuit current and the dark saturation current. This can be extended to relate V_{oc} to the photovoltaic gap E_{PVG} of the

solar cell by inserting the following expression into Eq. 4:[31]

$$j_0 = j_{00} \cdot \exp\left(\frac{-E_{\mathrm{PVG}}}{k_{\mathrm{B}}T}\right) \tag{6}$$

Here j_{00} denotes the coupling factor that is generally assumed to be a constant accounting for the electronic coupling strength of the material system[17,18,32,33]and E_{PVG} denotes the energy gap across which electrons and holes recombine. Note that j_{00} as defined by Eq. 6 also includes the dependence of the electronic coupling on the interfacial area in a heterojunction device. However, if devices with similar interface morphology are compared, it directly reflects the different electronic coupling of donor and acceptor molecules. Under the assumption $j_{\mathrm{sc}}/j_0 \gg 1$, Eq.4 and Eq.6 yield the commonly found relation[15,31,34]:

$$qV_{\mathrm{oc}} \approx E_{\mathrm{PVG}} - k_{\mathrm{B}}T \cdot \ln\left(\frac{j_{00}}{j_{\mathrm{sc}}}\right). \tag{7}$$

Equation 7 implies a linear temperature dependence of the V_{oc}, which approaches a value of E_{PVG}/q at absolute zero. A linear extrapolation to 0 K of the V_{oc} measured at a series of temperatures is thus widely used in order to experimentally determine E_{PVG}.[8,11,18,19] In the context of organic heterojunction solar cells E_{PVG} is oftentimes identified with the energy of the charge transfer state E_{CT}, even though various terms for slightly different experimental conditions are used.[8,18,19,32,33,35,36] It is important to note that this identification is *not a priori* made here.

Simulated temperature dependences of the open circuit voltage (calculated by Eq. 4) for a broad range of α_{CT} are shown in Figure 2 (a). Values of $E_{\mathrm{opt}} = 2.1\,\mathrm{eV}$ and $E_{\mathrm{CT}} = 1.8\,\mathrm{eV}$ have been chosen, corresponding to a heterojunction of α-sexithiophene (6T) and diindenoperylene (DIP) as determined by Hörmann *et al.* and Wilke *et al.*[15,36]. As was already shown by Gruber *et al.* for DIP/C_{60} solar cells, the V_{oc} indeed shows an approximately linear temperature dependence down to 0 K for high α_{CT} values, while for very low α_{CT} the open circuit voltage at finite temperature may exceed E_{CT}/q. In the extreme case of $\alpha_{\mathrm{CT}} = 0$ (dashed line Figure 2 (a)) the device behaves like a classical homojunction with a band gap of 2.1 eV.[8]

In order to understand the occurrence of the kink of V_{oc} observed for low α_{CT} values, we have to take a closer look into Eq. 3 and Eq. 1. For a bi-step function as given by Eq. 2 the

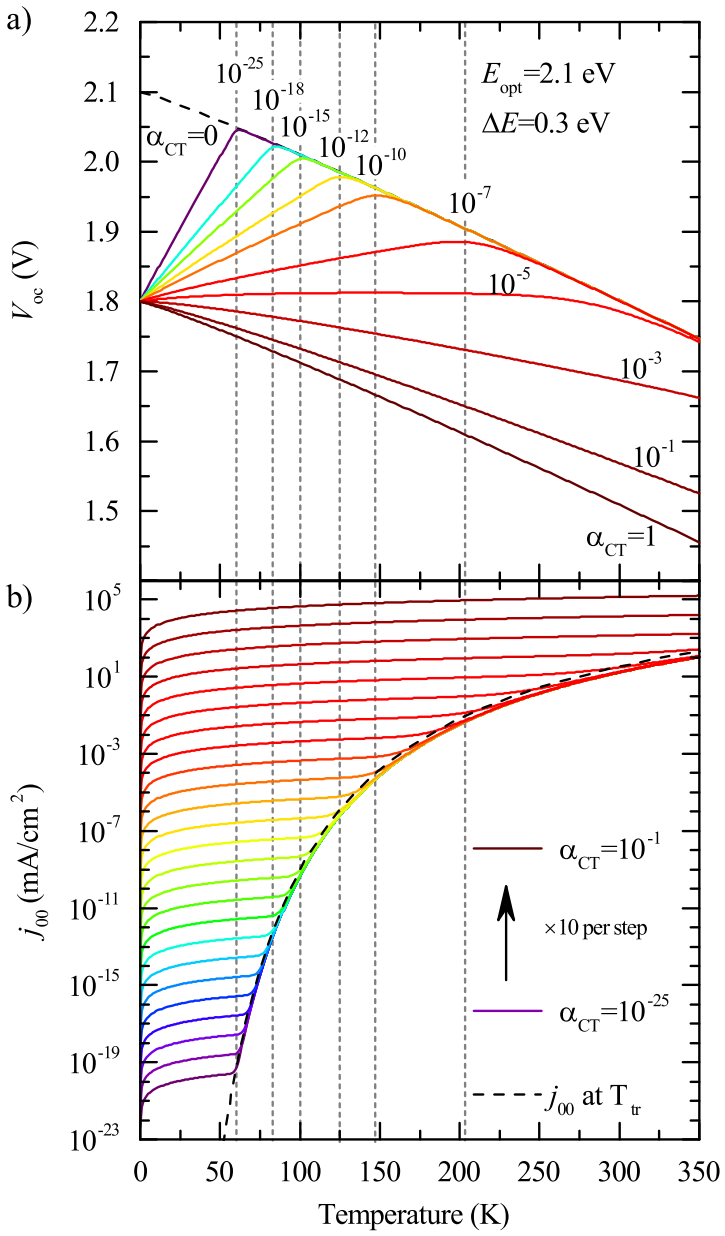

FIG. 2: Simulation of the temperature dependence of the open circuit voltage (a) and the coupling factor (b) of an ideal solar cell for a variation of α_{CT}. E_{opt} and ΔE have been chosen to match the material system 6T/DIP. For calculation of V_{oc} from Eq. 4, the short circuit current was calculated from the spectrum of a black body at the temperature of the sun. For clarity, only a subset of the α_{CT} values is shown in (a). The transition temperature for this subset is indicated by vertical, dashed lines.

integral can be solved analytically and yields:

$$\begin{aligned} N(T) =& Ak_{\mathrm{B}}T\left[\alpha_{\mathrm{CT}}\,\xi_{\mathrm{CT}}(T)\exp\left(\frac{-E_{\mathrm{CT}}}{k_{\mathrm{B}}T}\right)+\right. \\ &\left.+(\alpha_0-\alpha_{\mathrm{CT}})\,\xi_{\mathrm{opt}}(T)\exp\left(\frac{-E_{\mathrm{opt}}}{k_{\mathrm{B}}T}\right)\right] \end{aligned} \tag{8}$$

where $A = 1/(4\pi^2\hbar^3c^2)$ and the parameters ξ_{CT} and ξ_{opt} are given by:

$$\begin{aligned} \xi_{\mathrm{CT}}(T) &= E_{\mathrm{CT}}^2 + 2k_{\mathrm{B}}TE_{\mathrm{CT}} + 2k_{\mathrm{B}}^2T^2 \\ \xi_{\mathrm{opt}}(T) &= E_{\mathrm{opt}}^2 + 2k_{\mathrm{B}}TE_{\mathrm{opt}} + 2k_{\mathrm{B}}^2T^2 \end{aligned} \tag{9}$$

And thus:

$$\begin{aligned} j_0 =& qAk_{\mathrm{B}}T\Bigg[\underbrace{\alpha_{\mathrm{CT}}\xi_{\mathrm{CT}}(T)}_{\text{emission via } E_{\mathrm{CT}}}+ \\ &+\underbrace{(\alpha_0-\alpha_{\mathrm{CT}})\xi_{\mathrm{opt}}(T)\exp\left(\frac{E_{\mathrm{CT}}-E_{\mathrm{opt}}}{k_{\mathrm{B}}T}\right)}_{\text{emission via } E_{\mathrm{opt}}}\Bigg]\cdot\exp\left(\frac{-E_{\mathrm{CT}}}{k_{\mathrm{B}}T}\right) \\ \equiv& j_{00}\cdot\exp\left(\frac{-E_{\mathrm{CT}}}{k_{\mathrm{B}}T}\right) \end{aligned} \tag{10}$$

This expression has the structure of Eq. 6, where E_{PVG} formally is identified with E_{CT}. Be aware that the factoring in Eq. 10 was an arbitrary choice. A similar expression can be derived that formally identifies E_{PVG} with E_{opt}. This does, however, not affect the general message of the following considerations.

In contrast to the common treatment (i.e. exploiting Eq. 6), this is utterly dependent on temperature as illustrated in Figure 2 (b). In particular, two terms with different temperature dependence can be identified. The first term is responsible for emission via the CT state, the second describes emission via the optical gap of the system. Depending on the temperature, one of the two terms is dominant, thus that a *transition temperature* T_{tr} can be defined as the temperature where both contributions are equal:

$$\alpha_{\mathrm{CT}}\xi_{\mathrm{CT}}(T_{\mathrm{tr}}) \stackrel{!}{=} (\alpha_0-\alpha_{\mathrm{CT}})\xi_{\mathrm{opt}}(T_{\mathrm{tr}})\exp\left(\frac{E_{\mathrm{CT}}-E_{\mathrm{opt}}}{k_{\mathrm{B}}T_{\mathrm{tr}}}\right) \tag{11}$$

This equation can only be solved numerically. However, for sufficiently low temperatures (typically below 2000 K) the parameters ξ reduce to $\xi_{\mathrm{CT}}(T) \approx E_{\mathrm{CT}}^2$ and $\xi_{\mathrm{opt}}(T) \approx E_{\mathrm{opt}}^2$

respectively and an analytical approximation of T_{tr} is possible:

$$T_{\mathrm{tr}} \approx \frac{\Delta E}{k_{\mathrm{B}}\left[\ln\left((\alpha_0 - \alpha_{\mathrm{CT}})E_{\mathrm{opt}}^2\right) - \ln\left(\alpha_{\mathrm{CT}}E_{\mathrm{CT}}^2\right)\right]} \tag{12}$$

where $\Delta E = E_{\mathrm{opt}} - E_{\mathrm{CT}}$ denotes the energy difference between the optical gap of the absorber and the CT energy. It is worth mentioning that the transition temperature does not depend on the choice of factoring in Eq. 10. It does, however, clearly depend on α_{CT} and ΔE. Figure 3 shows this dependency and additionally illustrates that the analytical approximation almost perfectly matches the numerical calculation of T_{tr} for practically relevant temperatures. In principle, T_{tr} not only depends on ΔE but also on the absolute values of E_{opt} and E_{CT}, yet their influence is small.

The transition temperature for the corresponding α_{CT} values is indicated as the vertical, dashed lines in Figure 2. It is clearly visible that T_{tr} marks the kink in both the V_{oc} and the j_{00} curves. The value of j_{00} at the respective transition temperature is indicated by the dashed curve in Figure 2 (b). The curve shapes are distinctly different left and right of the transition temperature and, except for a small transition region, the coupling is clearly dominated by the contribution of recombination either via the CT ($T < T_{\mathrm{tr}}$) or via the optical ($T > T_{\mathrm{tr}}$) gap. From Figure 2 (a) it becomes now obvious that a linear extrapolation of the V_{oc} at temperatures larger than T_{tr} will result in a photovoltaic gap that is close to E_{opt}. If V_{oc} values below T_{tr} are extrapolated, a value of $E_{\mathrm{PVG}} \approx E_{\mathrm{CT}}$ will be extracted.

Mathematically, this can be derived if Eq. 10 is considered in the respective temperature regime:

$$j_0 \approx \begin{cases} qAk_{\mathrm{B}}T\alpha_{\mathrm{CT}}\xi_{\mathrm{CT}}(T)\exp\left(\frac{-E_{\mathrm{CT}}}{k_{\mathrm{B}}T}\right) & : T < T_{\mathrm{tr}} \\ qAk_{\mathrm{B}}T(\alpha_0 - \alpha_{\mathrm{CT}})\xi_{\mathrm{opt}}(T)\exp\left(\frac{-E_{\mathrm{opt}}}{k_{\mathrm{B}}T}\right) & : T > T_{\mathrm{tr}} \end{cases} \tag{13}$$

Together with Eq. 4, this yields:

$$qV_{\mathrm{oc}} \approx \begin{cases} E_{\mathrm{CT}} - k_{\mathrm{B}}T \cdot \ln\left(\frac{j_{00}}{j_{\mathrm{sc}}}\right) & : T < T_{\mathrm{tr}} \\ E_{\mathrm{opt}} - k_{\mathrm{B}}T \cdot \ln\left(\frac{j_{00}}{j_{\mathrm{sc}}}\right) & : T > T_{\mathrm{tr}} \end{cases} \tag{14}$$

Thus, comparison to Eq. 7 shows that the identification of E_{PVG} with either E_{CT} or E_{opt}, cannot generally be made but depends on the temperature regime the solar cell is operated in. Please note that j_{00} as used in Eqs. 14 and 13 still contains a slight temperature dependence,

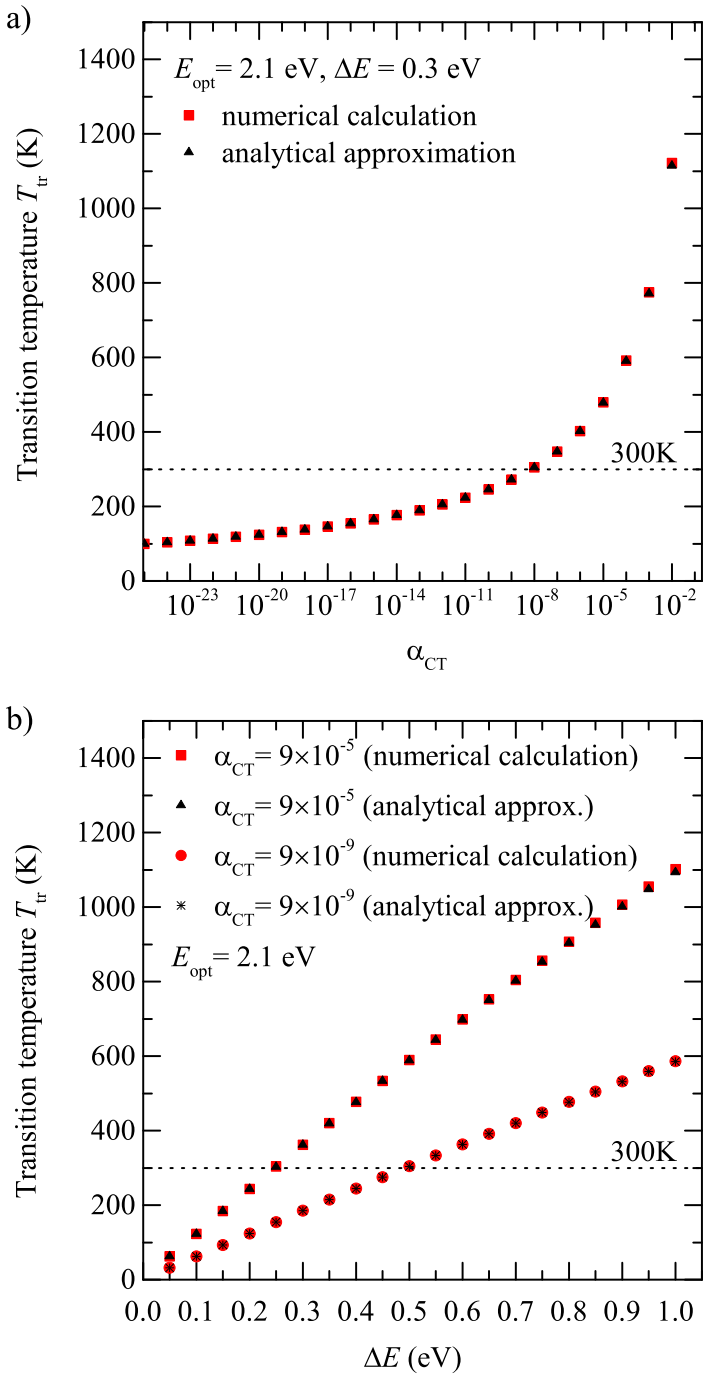

FIG. 3: Dependence of the transition temperature on α_{CT} (a) and ΔE (b) for values of E_{opt}, ΔE and α_{CT} that match the material system 6T/DIP.

which leads to a minor overestimation of E_{PVG} if the temperature dependence of V_{oc} is linearly extrapolated to 0 K, as shown by Gruber *et al.*.[8]

A second method to determine E_{PVG} arises from Eq. 6, that can be rewritten as:

$$\ln(j_0) = \frac{-E_{\mathrm{PVG}}}{k_{\mathrm{B}}T} + \ln(j_{00}) \tag{15}$$

E_{PVG} can then be extracted from the slope, if $\ln(j_0)$ is plotted against $\frac{1}{k_{\mathrm{B}}T}$. But depending on the temperature regime that is considered, this yields E_{CT} for $T < T_{\mathrm{tr}}$ and E_{opt} for $T > T_{\mathrm{tr}}$.

Recent publications identify E_{PVG} with E_{CT} for a broad range of material systems[11,18,19,33,35–37]. This implies that the transition temperature is above the typical operating temperature for the vast majority of real solar cell devices. Still, this is not necessarily the case for all solar cells and we will later show that for 6T/DIP devices this critically depends on the substrate temperature during 6T evaporation and thus the morphology at the interface between donor and acceptor.

C. Non-radiative recombination

So far, only ideal solar cells in the radiative limit have been discussed. Recombination in real devices, however, can usually not simply be described by radiative recombination of free charge carriers any more. Instead, non-radiative recombination processes play an important or even dominant role. In the simulations by Gruber *et al.* this was successfully accounted for by the introduction of a constant $\gamma = j_{0,\mathrm{non}}/j_{0,\mathrm{rad}}$ that linearly connects the non-radiative recombination to the radiative recombination current.[8]

Yet, if different recombination pathways have to be considered in the respective temperature regime the introduction of a single constant is insufficient to account for the fundamentally different processes. Hence, two constants γ_{CT} and γ_{opt} are introduced, corresponding to the non-radiative losses across the intermolecular gap and the optical gap of the absorber, respectively. The coupling factor j_{00} in Eq. 10 then reads:

$$\begin{aligned} j_{00} =& qAk_{\mathrm{B}}T\Big[(1+\gamma_{\mathrm{CT}})\alpha_{\mathrm{CT}}\xi_{\mathrm{CT}}(T) + (1+\gamma_{\mathrm{opt}})\cdot \\ & \cdot(\alpha_0 - \alpha_{\mathrm{CT}})\xi_{\mathrm{opt}}(T)\exp\left(\frac{E_{\mathrm{CT}} - E_{\mathrm{opt}}}{k_{\mathrm{B}}T}\right)\Big] \end{aligned} \tag{16}$$

Obviously, unequal non-radiative recombination losses, will change the transition tem-

perature compared to the ideal case, where larger values of one γ with respect to the other will favour the respective process:

$$T_{\mathrm{tr}} \approx \frac{\Delta E}{k_{\mathrm{B}}\left[\ln\left(\frac{(\alpha_0-\alpha_{\mathrm{CT}})E_{\mathrm{opt}}^2}{\alpha_{\mathrm{CT}}E_{\mathrm{CT}}^2}\right)+\ln\left(\frac{1+\gamma_{\mathrm{opt}}}{1+\gamma_{\mathrm{CT}}}\right)\right]} \tag{17}$$

For example $\gamma_{\mathrm{CT}} > \gamma_{\mathrm{opt}}$ will increase T_{tr} and hence increase the temperature range in which recombination across the CT state is dominant and vice versa.

III. EXPERIMENTAL INVESTIGATION

A. Temperature dependence of the open circuit voltage

In the following we focus on planar heterojunction (PHJ) solar cells of the material system 6T/DIP. The one and only difference between the two devices considered here is the substrate temperature during the evaporation of the 6T layer. While in the high temperature (HT) device the substrate was heated to 100 °C during 6T deposition, for the room temperature (RT) device the substrate temperature was not influenced. This leads to an increase of V_{oc} from 1.22 V for the RT device to 1.35 V for the HT device.[14,15] By investigation of the dark *j-V* characteristics Hörmann *et al.* have shown that the higher V_{oc} of the HT device comes in spite of enhanced recombination caused by a slight increase of the interfacial area, as indicated by a somewhat larger reverse saturation current j_0.[15] Obviously however, this effect is overcompensated by the different intermolecular coupling in both devices, as will be discussed in detail below.

The temperature dependent measurements of V_{oc} together with the linear extrapolation of this data to 0 K (green dashed line) are shown in the upper part of Figure 4. Although the same material combination for both cells is used, clearly two different values are obtained for the linear extrapolation of the respective measured V_{oc} data. For the RT device the value of E_{PVG} =1.9 eV is within the error identical to the intermolecular gap of 1.80 ± 0.15 eV as determined by photoelectron spectroscopy.[36] In contrast, for the HT device the determined value is clearly larger (E_{PVG} =2.07 eV), although UPS measurements did not indicate any changes of the interfacial energy level alignment resulting from different preparation conditions. Noteworthy, E_{PVG} is remarkably close to the optical gap of DIP (E_{opt} =2.1 eV).[38]

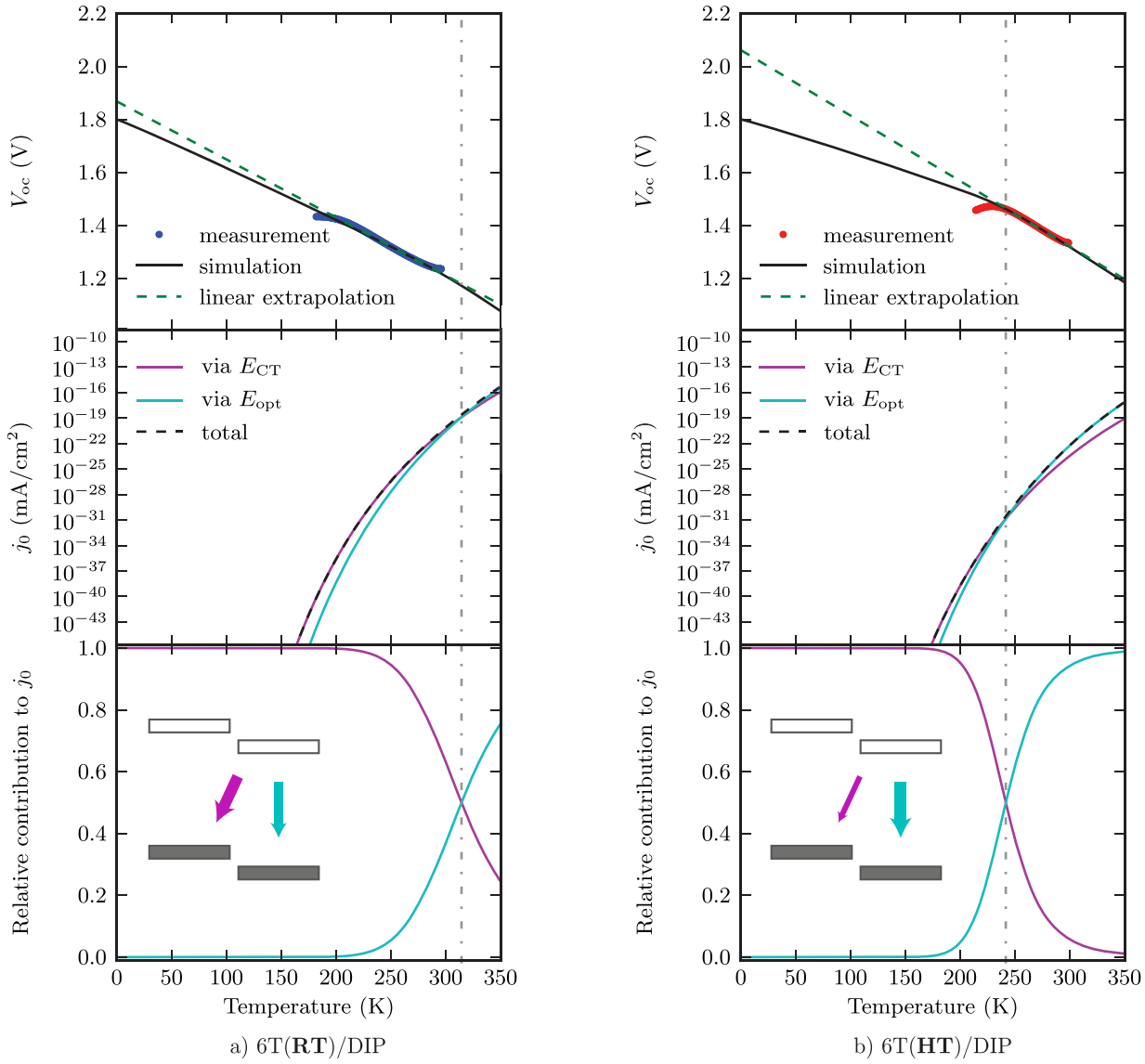

FIG. 4: Simulation of the temperature dependent open circuit voltage of 6T/DIP solar cells. The room temperature device is shown in (a), the solar cell with 6T grown at a substrate temperature of 100 °C in (b). The parameters used were $E_{opt} = 2.1$, $E_{CT} = 1.8$ for both cells, $\alpha_{CT} = 9 \times 10^{-5}$, $\gamma_{CT} = 7 \times 10^{7}$ and $\gamma_{opt} = 3 \times 10^{8}$ for the RT case, $\alpha_{CT} = 9 \times 10^{-8}$, $\gamma_{CT} = 5 \times 10^{7}$ and $\gamma_{opt} = 6 \times 10^{6}$ for the 6T(HT)/DIP device. The dash-dotted vertical lines mark the respective transition temperatures T_{tr}. The insets in the lowest graph illustrate the situation at 300 K.

Additionally, the temperature dependence of the open circuit voltage of both devices can be simulated with identical optical and intermolecular gaps regardless of the preparation conditions, but different parameters α_{CT}, γ_{CT} and γ_{opt}. The resulting curves for $E_{opt} = 2.1$ eV and $E_{CT} = 1.8$ eV are also displayed in the the upper part of Figure 4 as black lines. Note that the simulation uses a purely thermodynamic model and does not

account for electrical properties such as injection barriers or carrier mobility. This implies that the flattening visible in the simulated V_{oc} is of potentially different nature than that occurring in the experiment. In particular the simulation shows the transition between the dominant parts of the competing recombination mechanisms via the optical gap for higher temperatures and the CT gap for low temperatures.

Simulating the temperature dependent open circuit voltage, the individual contributions of CT and singlet recombination to the dark saturation current j_0 can be regarded separately (see Figure 4). The relative strength of the loss channels extracted from these simulations clearly confirm that neither the CT ($j_{0,CT}$) nor the singlet recombination ($j_{0,opt}$) component are completely negligible for the dark saturation current of both 6T/DIP devices (lowest graph in Figure 4). Yet, while the CT contribution dominates through the whole measured temperature range for the RT device, singlet recombination is predominant for the HT prepared solar cell in the relevant operating temperature regime. This is also visible in the total dark saturation current which clearly follows the curve of $j_{0,opt}$ right and $j_{0,CT}$ left of the transition temperature, indicated by the vertical dashed-dotted line in Figure 4.

Special conditions, under which recombination from the charge transfer state is of minor importance for the operating solar cell, have been predicted even for organic heterojunctions, if the energy of the CT state gets close to the energy of the optical gap of the absorber, or if the absorption strength of the CT state becomes extremely low.[6–8,39] In electro- and photoluminescence significant contribution from emission of the singlet state of the absorber has been observed experimentally for polymer/fullerene bulk heterojunction cells in a systematic variation of ΔE by carefully choosing the different donor/acceptor combinations. As reported by Faist *et al.*, activation of the singlet state from the CT state opened an additional recombination channel, if ΔE was less than 0.35 eV. With further reduction of ΔE, the recombination via this channel was significantly increased.[12]

In the present case of the 6T/DIP system, ΔE is about 0.3 eV and is thus close to the threshold energy found by Faist *et al.* below which singlet emission becomes activated. In our solar cells, however, the situation is somewhat different to the experiments performed by Faist *et al.* as the energetics at the interface stay the same for the different growth conditions. Since neither the intermolecular energy gap, nor the optical gap of the absorber change, ΔE is expected to remain identical and unchanged for both 6T/DIP cells. It is rather the intermolecular electronic coupling that appears to be reduced by the morphological changes,

if 6T is grown at 100 °C – most likely because of a reduction of the mutual face-on molecular orientation as a consequence of the absence of the lying/lying configuration in this device.[15] This leads to the situation that, while recombination via the optical gap of DIP is activated as a result of the low ΔE for both solar cells, CT recombination is hampered by the reduced intermolecular coupling for the HT device.

Yet, direct spectroscopic evidence following the example of Faist *et al.*[12] and Ran *et al.*[13] is required to strengthen the picture presented above.

B. Spectroscopic evidence for different recombination channels

Temperature dependent electroluminescence (EL) spectroscopy has been performed on both types of 6T/DIP devices as well as on single layers of DIP and 6T, respectively. The corresponding spectra at room temperature are shown in Figure 5. Since the architecture of all four devices is the same, higher voltages have to be chosen to obtain well resolved spectra for the single layers as the contacts are not optimised for these devices. For all spectra a Gaussian decomposition has been performed to examine the individual contributions to each spectrum. The peak positions are summarized in Table I. For both 6T/DIP devices singlet emission is observed even for voltages only slightly above V_{oc}. Comparing the peak positions of the emission spectra of both heterojunctions with the spectra of the single, neat layers of DIP and 6T one can conclude that singlet emission stems only from the DIP in both PHJs, and no emission from 6T is observed. As DIP has the smaller optical gap of both materials ($E_{\mathrm{opt,DIP}} = 2.1\,\mathrm{eV}$[38], $E_{\mathrm{opt,6T}} = 2.4\,\mathrm{eV}$[40]), this gap is the relevant optical gap of the system in the simulations presented above. However, the spectrum of the RT device cannot be fitted properly without the use of an additional Gaussian at an energy of 1.82 eV. Evidently, this peak can neither be attributed to 6T nor DIP (see Table I) and hence is assigned to the transition from the interfacial CT state to the ground state. Therefor these measurements strongly support the results of the simulations, namely that concerning the radiative contribution to j_0 at room temperature, recombination almost exclusively occurs via the optical gap for the HT device, whereas in the RT device, where the transition temperature is higher, recombination via the CT and the optical gap are detectable.

Similar observations can be made in Figure 6a) for the temperature dependent spectra of both solar cells at 300 K. Note, that all spectra are normalized to their maximum. Although

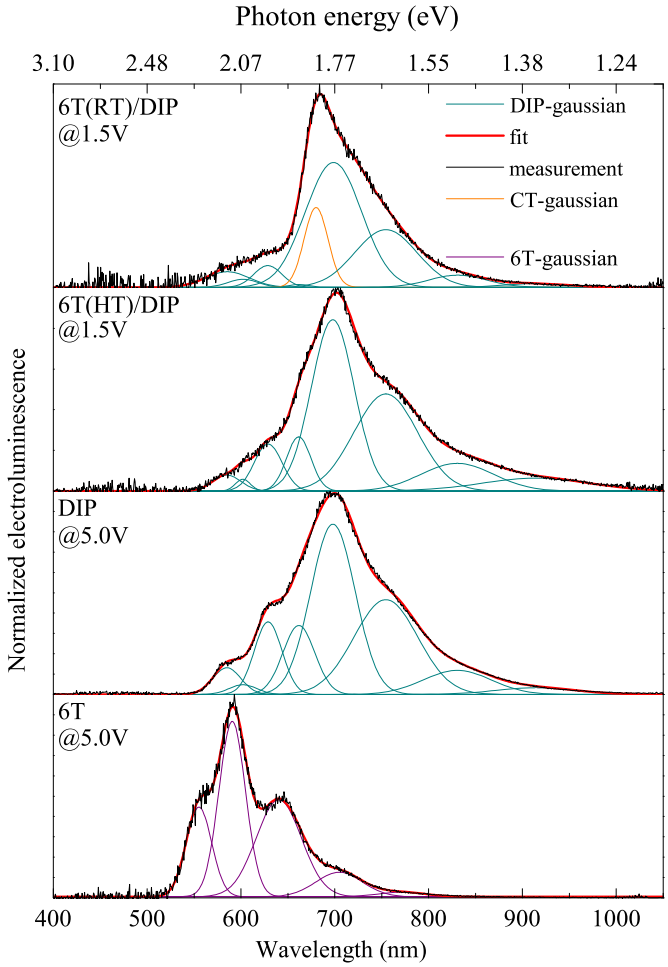

FIG. 5: Measured electroluminescence spectra (black curves) of RT- and HT-6T/DIP solar cells for an applied voltage of 1.5 V together with the Gaussian decomposition (red curve). In the lower part electroluminescence spectra of DIP- and 6T-single layers at room temperature and an applied voltage of 5.0 V are shown.

the applied voltage is now 5.0 V, the spectrum of the HT device shows strong contributions from the DIP signal, whereas in the RT cell this emission is strongly suppressed but followed by a strong emission peak at about 1.8 eV.

Reducing the temperature leads to strong changes in the spectra of both devices. Most remarkably the strong contribution of the DIP emission in the HT devices is largely attenuated with reduced temperature. This transition again is an observation that has been predicted by the simulations discussed above. When operated at 300 K this device is far above its transition temperature, so that reducing the temperature brings the device closer to T_{tr}, where the recombination via the CT gap increases. However, further reduction of the

TABLE I: Peak positions of DIP and 6T single layers as well as RT and HT 6T/DIP devices as obtained by fitting the measured spectra with Gaussians. The peak centered at 680 nm (= 1.82 eV) cannot be attributed to any of the neat materials and is thus considered as emission from the CT state.

Device	**Peak position (nm)**									
6T	555.2	590.7		640.3			704.7	771.3		
DIP		585.0	602.1	628.9	661.7	698.0		754.4	830.5	914.6
6T/DIP (HT)		585.0	602.0	628.9	661.5	697.8		754.4	830.5	914.0
6T/DIP (RT)		585.5	602.3	628.6	661.7	**680.0**	698.6	754.5	830.9	914.1

temperature does not lead to the pure CT signal, as expected from the simulations. Already at 200 K new features arise in the HT device spectrum between 550 and 715 nm, which also become visible in the RT device spectrum at lower temperatures. To be able to understand this apparent discrepancy, the temperature dependent characteristics of both single layer devices have to be considered. These spectra are shown in Figure 6 b) and c) for DIP and 6T single layers, respectively. For both materials strong temperature dependence of the EL spectra is observed.

In the 6T spectrum the five dominant peaks at room temperature (marked by solid vertical lines) strongly decrease by lowering the temperature. Already at a temperature of 200 K new features arise that completely dominate the spectrum at 150 K and lower temperatures. The positions of the dominant features in the low temperature spectra are marked by dashed lines. To fit the spectra at 50 K eight Gaussians were needed (not shown here). By comparing the peak positions at 50 K with the ones at room temperature (see Figure 5) it becomes obvious that some of the room temperature peaks are still present in the 50 K spectrum, but relatively weak. The peak at 555.2 nm (2.23 eV) completely vanishes for low temperatures. Similar observations have been made in literature for photoluminescence spectra,[41–45] where the temperature dependence has been attributed to the presence of aggregate states. This phenomenon is then explained as photoexcitations that are trapped by low lying aggregate states for all temperatures, but at low temperatures the backscattering to the higher energy exciton states is hindered and photoluminescence originates solely from the aggregate electronic levels. As temperature approaches room temperature, the probability for the trapped photoexcitations to backscatter to the exciton level within their lifetime increases and the exciton level becomes the predominant radiative channel.[42,43]

Similar temperature dependent spectra are observed for DIP. Again the first peak at 585.0 nm disappears with decreasing temperature and below 150 K new features completely dominate the spectrum of the DIP single layer. Fitting the spectra at 300 K and at 50 K with Gaussians again leads to the observation that some of the room temperature peaks are still present at 50 K. The positions of the peaks, that are only present at low temperatures are marked with cyan dashed lines. Unfortunately, there is only limited literature data available on the temperature dependence of DIP spectra. Heilig *et al.* performed time and temperature dependent fluorescence spectroscopy and observed three different line series with different time and temperature dependence. In the slow time window and at low temperatures a clear doublet splitting has been identified that has its spectral signature at 595 nm and 604 nm, but for higher temperatures both signals disappear.[46] This can be confirmed by our electroluminescence spectra, where these two peaks also can be found for low temperatures only. Heilig *et al.* assigned these two signals to trap states.

The important peak positions for both materials, 6T and DIP, are also indicated in Figure 6a) as a guide for the eye. With the help of these lines and arrows it becomes obvious that the new arising features for both spectra at low temperatures are due to the changes in the emission spectra of both individual materials. Localized emission of DIP as well as of 6T can be observed in both, the RT and the HT device spectra for temperatures lower than 200 K. Furthermore, a slight shift in the position of the absolute maximum to higher energies can be identified for both devices with decreasing temperature, so that at 50 K the maxima of both spectra coincide with the third low temperature emission peak of 6T. From these spectra it can be assumed that emission via aggregate or trap states is the dominant radiative recombination path at low temperatures. This may be due to the fact that these states lie energetically even below the interfacial CT state. While at higher temperatures the thermal energy is high enough to reach the CT state or even the singlet state, at low temperatures charge carriers are trapped in these deep lying states and emission occurs exclusively from these states. This makes it impossible to observe the exact transition temperature for the HT device, because the CT emission is not dominating the spectra for low temperatures as predicted by the presented model using a simplified absorption spectrum.

Nevertheless, these spectra strongly support the existence of a transition temperature as predicted by the model presented in the first part, especially for temperatures between 300 K and 200 K. In this temperature range for the HT device only emission from the optical gap

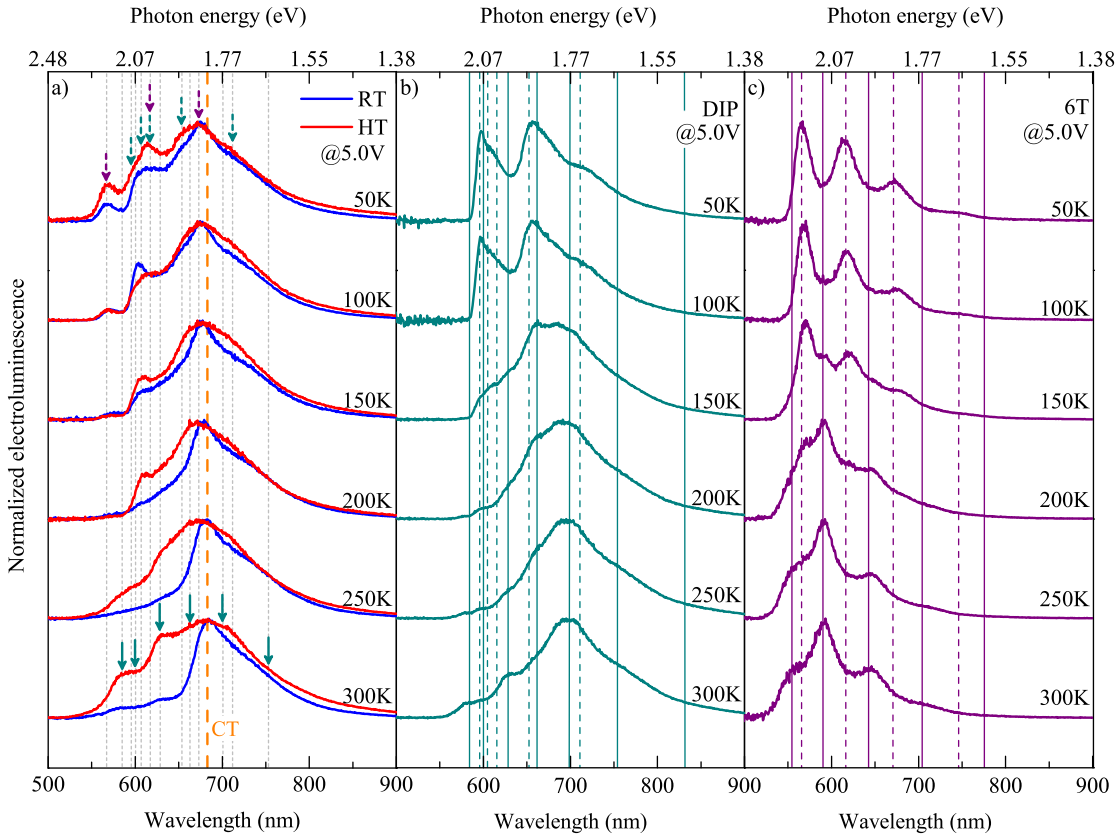

FIG. 6: Temperature dependent electroluminescence spectra for HT and RT 6T/DIP solar cells (red and blue, respectively)(a) and DIP- (b) and 6T-single layer cells (c). All spectra have been measured at an applied voltage of 5.0 V. Vertical solid lines and arrows mark peak position that are present at room temperature, whereas vertical dashed lines and arrows indicate peaks that appear at lower temperatures. The orange dashed line marks the position of the CT-peak as determined in Figure 5.

of DIP is observed, whereas for the RT device additional recombination via the CT gap can be detected.

IV. CONCLUSION

In conclusion, a modification of the Shockley-Queisser theory for organic heterojunctions, which was previously reported in the literature,[8] has been presented with a special focus on constellations, where a linear extrapolation of the predicted open circuit voltage would result in the optical gap of the absorber rather than in the intermolecular charge transfer energy gap. This behaviour has been observed for 6T/DIP devices, where temperature dependent device characteristics indicate different photovoltaic energy gaps for the room temperature

and the high temperature grown device. A temperature dependent competition between the recombination via the CT gap and the optical gap of the absorber has been identified as the cause. Therefor a transition temperature T_{tr} was introduced, that separates temperature regimes where recombination across the charge transfer gap ($T < T_{\mathrm{tr}}$) and the optical gap ($T > T_{\mathrm{tr}}$) dominates. This transition temperature depends on the coupling between donor and acceptor molecules at the interface as could be shown for 6T/DIP devices. For these solar cells the small energy offset of $\Delta E \approx 0.3\,\mathrm{eV}$ activates singlet emission as a relevant recombination channel and, as a consequence, shifts the transition temperature towards lower temperatures and hence closer to the actual operation temperature. Preparation of the 6T film at an elevated substrate temperature changes the film morphology in such a way that the overall intermolecular coupling at the donor/acceptor interface is reduced while the offset energy ΔE remains constant. This leads to a reduction of the transition temperature below the operation temperature of the solar cell, which renders recombination across the optical gap of the absorber the dominant recombination channel. As a consequence, the linear extrapolation of temperature dependent V_{OC} measurements towards 0 K results in the energy of the optical gap E_{opt} rather than the charge transfer energy E_{CT} for this device.

Temperature dependent electroluminescence spectroscopy confirms the contribution of E_{opt} for both devices. For 300 K and low voltages the HT device indeed shows exclusively DIP emission whereas the RT cell spectrum can only be fitted by the use of an additional Gaussian that is attributed to the emission from the interfacial CT state. This CT emission is accompanied by a strongly reduced emission from DIP in comparison to the HT sample, as predicted by the simulations. Reducing the temperature to 200 K leads to strongly reduced DIP emission in case of the HT device, as the device is brought closer to its transition temperature. However, reducing the temperature further does not lead to pure CT emission for both cells, since new features are arising. With the help of temperature dependent spectra of both single materials, these features could be attributed to the emission of aggregate states in the single materials that dominate the spectra for low temperatures. Nevertheless the existence of the transition temperature T_{tr} could be confirmed. Yet, for most solar cells T_{tr} is much higher than 300 K and thus does not influence normal operation. But for devices with small energy offset ΔE and weak intermolecular coupling the transition temperature T_{tr} might be in the range of typical operation temperatures. This also implies, that extrapolation of temperature dependent V_{OC} measurements to 0 K to determine the

charge transfer energy E_{CT} has to be handled with care as it might in some cases deliver the optical gap E_{opt} of one of the absorbers.

V. EXPERIMENTAL DETAILS

Sample preparation: Organic solar cells were fabricated on commercially available indium-tin oxide (ITO) coated glass substrates (purchased from Thin Film Devices, Inc., Anaheim, CA; sheet resistance $\approx 20\,\Omega$/square). Prior to the evaporation of the active organic layers, a 30 nm thick layer of poly(3,4-ethylenedioxythiophene):poly(styrenesulfonate) (PEDOT:PSS; purchased from Heraeus Clevios GmbH, Leverkusen, Germany) was spin coated from an aqueous solution and annealed at 125 °C for 30 min on a hot plate under ambient conditions. Subsequently, the active donor and acceptor layers as well as a 5 nm layer of the exciton blocking material bathocuproine (BCP; purchased from Sigma Aldrich as sublimed grade and used without further purification) were deposited using a standard thermal evaporation procedure at base pressures of 10^{-7}mbar. Finally, 100 nm of aluminium were evaporated through a shadow mask as a top electrode, resulting in an active area of $A = 4\,\mathrm{mm}^2$. Thus the layer sequence for all devices is: ITO/PEDOT:PSS/organic layers/BCP/Al. The active materials, diindenoperylene (DIP; purchased from S. Hirschmann, University of Stuttgart, Stuttgart, Germany) and α-sexithiophene (6T; purchased from Sigma Aldrich), were purified twice by gradient sublimation.

Temperature dependence of the open circuit voltage: Temperature dependent measurements of V_{oc} were recorded in a continuous flow liquid nitrogen cryostat (CryoVac). The solar cells were illuminated with a simulated AM1.5G spectrum at an intensity of roughly one sun.

Electroluminescence measurements: Electroluminescence (EL) measurements were carried out by using a liquid-nitrogen-cooled CCD camera (PyLoN:100BR_ eXcelon, Princton Instruments) coupled with a spectrometer (SP2300i, Princton Instruments) with a spectral sensitivity in the wavelength range of approximately 300-1000 nm. The measurements were performed under a dc voltage drive from a Keithley source meter. The samples were transfered into a liquid-helium-cooled cryostat (Cryovac) with an inert gas atmosphere (approximately 300 mbar He) without air exposure.

VI. AKNOWLEDGEMENT

This work was funded by the German Research Foundation (DFG) within the priority program SPP1355 "Elementary Processes of Organic Photovoltaics" and by the Bavarian State Ministry of Science, Research and the Arts within the collaborative research network "Solar Technologies go Hybrid". U.H. and S. G. thank the Bavarian Research Foundation (BFS) for PhD scholarships.

---

* wolfgang.bruetting@physik.uni-augsburg.de

[1] "Heliatek GmbH. Heliatek reaches efficiency record with 40 % transparent organic solar cells (Press release March 24, 2014). (http://www.heliatek.com/de/news/news/details/heliatek-erzielt-effizienzrekord-mit-40-transparenten-organischen-solarzellen-111)," (2014).

[2] "Heliatek GmbH. Asias largest Building Integrated Organic PV (BIOPV) First installation of HeliaFilm® completed in Singapore (Press release September 14, 2015). (http://www.heliatek.com/en/press/press-releases/details/asias-largest-building-integrated-organic-pv-biopv-first-installation-of-heliafilm-completed-in-singapore)," (2015).

[3] http://www.nrel.gov/ncpv/.

[4] M. A. Green, K. Emery, Y. Hishikawa, W. Warta, and E. D. Dunlop, Progress in Photovoltaics: Research and Applications **23**, 805 (2015).

[5] R. A. J. Janssen and J. Nelson, Advanced Materials **25**, 1847 (2013).

[6] N. C. Giebink, G. P. Wiederrecht, M. R. Wasielewski, and S. R. Forrest, Physical Review B **83**, 195326 (2011).

[7] L. J. A. Koster, S. E. Shaheen, and J. C. Hummelen, Advanced Energy Materials **2**, 1246 (2012).

[8] M. Gruber, J. Wagner, K. Klein, U. Hörmann, A. Opitz, M. Stutzmann, and W. Brütting, Advanced Energy Materials **2**, 1100 (2012).

[9] J.-L. Brédas, J. E. Norton, J. Cornil, and V. Coropceanu, Accounts of Chemical Research **42**, 1691 (2009).

[10] K. Tvingstedt, K. Vandewal, A. Gadisa, F. Zhang, J. Manca, and O. Inganäs, Journal of the American Chemical Society **131**, 11819 (2009).

[11] K. Vandewal, K. Tvingstedt, A. Gadisa, O. Inganäs, and J. V. Manca, Physical Review B **81**, 125204 (2010).

[12] M. A. Faist, T. Kirchartz, W. Gong, R. S. Ashraf, I. McCulloch, J. C. de Mello, N. J. Ekins-Daukes, D. D. C. Bradley, and J. Nelson, Journal of the American Chemical Society **134**, 685 (2012).

[13] N. A. Ran, M. Kuik, J. A. Love, C. M. Proctor, I. Nagao, G. C. Bazan, and T.-Q. Nguyen, Advanced Materials **26**, 7405 (2014).

[14] U. Hörmann, J. Wagner, M. Gruber, A. Opitz, and W. Brütting, physica status solidi (RRL) - Rapid Research Letters **5**, 241 (2011).

[15] U. Hörmann, C. Lorch, A. Hinderhofer, A. Gerlach, M. Gruber, J. Kraus, B. Sykora, S. Grob, T. Linderl, A. Wilke, A. Opitz, R. Hansson, A. S. Anselmo, Y. Ozawa, Y. Nakayama, H. Ishii, N. Koch, E. Moons, F. Schreiber, and W. Brütting, Journal of Physical Chemistry C **118**, 26462 (2014).

[16] Y. Yi, V. Coropceanu, and J.-L. Brdas, Journal of the American Chemical Society **131**, 15777 (2009).

[17] K. R. Graham, P. Erwin, D. Nordlund, K. Vandewal, R. Li, G. O. Ngongang Ndjawa, E. T. Hoke, A. Salleo, M. E. Thompson, M. D. McGehee, and A. Amassian, Advanced Materials **25**, 6076 (2013).

[18] U. Hörmann, J. Kraus, M. Gruber, C. Schuhmair, T. Linderl, S. Grob, S. Kapfinger, K. Klein, M. Stutzman, H. Krenner, and W. Brütting, Physical Review B **88**, 235307 (2013).

[19] J. Widmer, M. Tietze, K. Leo, and M. Riede, Advanced Functional Materials **23**, 5814 (2013).

[20] W. Shockley and H. J. Queisser, Journal of Applied Physics **32**, 510 (1961).

[21] T. Kirchartz, J. Mattheis, and U. Rau, Physical Review B **78**, 235320 (2008).

[22] T. Kirchartz, K. Taretto, and U. Rau, The Journal of Physical Chemistry C **113**, 17958 (2009).

[23] G. Kirchhoff, Annalen der Physik **185**, 275 (1860).

[24] P. Würfel, *Physics of Solar Cells: From Basic Principles to Advanced Concepts*, 2nd ed. (Wiley-VCH Verlag, Weinheim, 2009).

[25] U. Rau, Physical Review B **76**, 085303 (2007).

[26] R. T. Ross, The Journal of Chemical Physics **46**, 4590 (1967).

[27] Y. Xu, T. Gaong, and J. N. Munday, Scientific Reports **5**, 13536 (2015).

[28] U. Rau, U. W. Paetzold, and T. Kirchartz, Phys. Rev. B **90**, 035211 (2014).

[29] A. Polman and H. A. Atwater, Nature Materials **11**, 174 (2012).

[30] M. Grätzel, Nature Materials **13**, 838 (2014).

[31] S. Sze and K. K. Ng, *Physics of Semiconductor Devices*, 3rd ed. (Wiley Interscience, New Jersey, 2006) p. 95.

[32] W. J. Potscavage, S. Yoo, and B. Kippelen, Applied Physics Letters **93**, 193308 (2008).

[33] M. D. Perez, C. Borek, S. R. Forrest, and M. E. Thompson, Journal of the American Chemical Society **131**, 9281 (2009).

[34] S. Yamamoto, A. Orimo, H. Ohkita, H. Benten, and S. Ito, Advanced Energy Materials **2**, 229 (2012).

[35] B. Rand, D. Burk, and S. Forrest, Physical Review B **75**, 115327 (2007).

[36] A. Wilke, J. Endres, U. Hörmann, J. Niederhausen, R. Schlesinger, J. Frisch, P. Amsalem, J. Wagner, M. Gruber, A. Opitz, A. Vollmer, W. Brütting, A. Kahn, and N. Koch, Applied Physics Letters **101**, 233301 (2012).

[37] D. Veldman, S. C. J. Meskers, and R. A. J. Janssen, Advanced Functional Materials **19**, 1939 (2009).

[38] U. Heinemeyer, R. Scholz, L. Gisslén, M. Alonso, J. Ossó, M. Garriga, A. Hinderhofer, M. Kytka, S. Kowarik, A. Gerlach, and F. Schreiber, Physical Review B **78**, 085210 (2008).

[39] J. Nelson, J. Kirkpatrick, and P. Ravirajan, Physical Review B **69**, 035337 (2004).

[40] P. I. Djurovich, E. I. Mayo, S. R. Forrest, and M. E. Thompson, Organic Electronics **10**, 515 (2009).

[41] A. Mani, J. Schoonman, and A. Goossens, The Journal of Physical Chemistry B **109**, 4829 (2005).

[42] P. Mei, M. Murgia, C. Taliani, E. Lunedei, and M. Muccini, Journal of Applied Physics **88**, 5158 (2000).

[43] R. N. Marks, M. Muccini, E. Lunedi, R. H. Michel, M. Murgia, R. Zamboni, C. Taliani, G. Horowitz, F. Garnier, M. Hopmeier, M. Oestreich, and R. F. Mahrt, Chemical Physics **227**, 49 (1998).

[44] M. Muccini, M. Murgia, and F. Biscarini, Advanced Materials **13**, 355 (2001).

[45] R. Capelli, C. Taliani, and M. Muccini, Synthetic Metals **139**, 691 (2003).

[46] M. Heilig, M. Domhan, and H. Port, Journal of Luminescence **110**, 290 (2004).